

# Behaviour of the Serre Equations in the Presence of Steep Gradients Revisited

J.P.A. Pitt<sup>a,\*</sup>, C. Zoppou<sup>a</sup>, S.G. Roberts<sup>a</sup>

<sup>a</sup>*Mathematical Sciences Institute, Australian National University, Canberra, ACT 0200, Australia*

---

## Abstract

*Keywords:* Serre equations, steep gradients, dam break

---

### 1. Serre Equations

2 The Serre equations can be derived by integrating the full incompressible Euler  
3 equations over the water depth [6]. They can also be derived as an asymptotic expansion  
4 of the Euler equations [7].

5 Assuming a constant horizontal bed the one-dimensional Serre equations are [8]

$$6 \quad \frac{\partial h}{\partial t} + \frac{\partial(uh)}{\partial x} = 0 \quad (1a)$$

8 and

$$9 \quad \underbrace{\frac{\partial(uh)}{\partial t} + \frac{\partial}{\partial x} \left( u^2 h + \frac{gh^2}{2} \right)}_{\text{Shallow Water Wave Equations}} + \underbrace{\frac{\partial}{\partial x} \left( \frac{h^3}{3} \left[ \frac{\partial u}{\partial x} \frac{\partial u}{\partial x} - u \frac{\partial^2 u}{\partial x^2} - \frac{\partial^2 u}{\partial x \partial t} \right] \right)}_{\text{Dispersion Terms}} = 0. \quad (1b)$$

10  $\overbrace{\hspace{25em}}$  Serre Equations

11 Where  $u(x, t)$  is the horizontal velocity over the depth of water  $h(x, t)$ ,  $g$  is the acceleration  
12 due to gravity,  $x$  is the horizontal spatial variable and  $t$  is time.

13 The Serre equations are conservation laws for mass ( $h$ ) and momentum ( $uh$ ) [6].  
14 The Serre equations admit a Hamiltonian [9, 10]

$$15 \quad \mathcal{H}(x, t) = \frac{1}{2} \left( hu^2 + \frac{h^3}{3} \left( \frac{\partial u}{\partial x} \right)^2 + gh^2 \right) \quad (2)$$

17 which represents the energy for the Serre equations and is also conserved.

---

\*Corresponding author

Email addresses: jordan.pitt@anu.edu.au (J.P.A. Pitt),  
christopher.zoppou@anu.edu.au (C. Zoppou), stephen.roberts@anu.edu.au  
(S.G. Roberts)

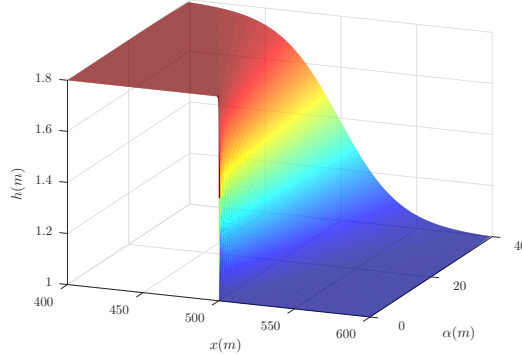


Figure 1: Initial conditions for the smooth dam-break problem with  $h_0 = 1m$ ,  $h_1 = 1.8m$  and  $x_0 = 500m$  as  $\alpha$  varies.

18     The total amount of a quantity  $q$  in a system occurring on the interval  $[a, b]$  is  
19     measured by

$$20 \quad C_q(t) = \int_a^b q(x, t) dx.$$

$$21$$

22     Conservation of a quantity  $q$  implies that  $C_q(0) = C_q(t) \forall t$  provided the interval is  
23     fixed and the system is closed. Our numerical methods should have this conservation  
24     property for  $h$ ,  $uh$  and  $\mathcal{H}$ .

25     **2. Smoothed Dam Break Problem**

26     In the literature the dam-break problem is approximated by a smooth hyperbolic  
27     tangent function [3, 4]. Such an approximation is called a smoothed dam-break prob-  
28     lem and is defined by

$$29 \quad h(x, 0) = h_0 + \frac{h_1 - h_0}{2} \left( 1 + \tanh \left( \frac{x_0 - x}{\alpha} \right) \right), \quad (3a)$$

$$30$$

$$31$$

$$32 \quad u(x, 0) = 0.0m/s \quad (3b)$$

$$33$$

34     where  $\alpha$  measures the distance over which approximately 46% of the smooth transition  
35     between the two heights of  $h_0$  and  $h_1$  centred around  $x_0$  occurs. Decreasing  $\alpha$  increases  
36     the steepness of the smoothed dam-break problem as can be seen in Figure 1 by varying  
37      $\alpha$  for different smoothed dam-break problems with fixed heights  $h_1 = 1.8m$  and  $h_0 =$   
38      $1m$  and fixed centre  $x_0 = 500m$ . These are the same  $h_0$  and  $h_1$  values as those of the  
39     dam-break problems of El et al. [1] and Le Métayer et al. [2] and will be the values  
40     used in Sections 2 and 4.

41    2.1. Assessing validity of Numerical Solutions

42    There are no analytic results for the Serre equations for either the discontinuous  
 43    dam-break problem or its smoothed approximation. To assess the validity of our nu-  
 44    merical solutions we use four comparisons. The first two investigate the behaviour  
 45    of the numerical solutions of our highest order method as  $\Delta x \rightarrow 0$  by measuring the  
 46    relative distance between solutions ( $L_1$ ) and the error in conservation ( $C_1$ ). The third  
 47    compares the numerical solutions of different methods when  $\Delta x$  is fixed. Lastly there  
 48    are also the Whitham modulation results of El et al. [1] who derived an expression  
 49    for the amplitude of the leading wave of an undular bore. If our numerical solutions  
 50    converged with small errors in conservation as  $\Delta x \rightarrow 0$ , agree with numerical solu-  
 51    tions from different methods and agree with the Whitham modulation results then our  
 52    numerical solutions are accurate approximate solutions of the Serre equations.

53    To compare the numerical solutions requires some notation around the spatial grids  
 54    defined by  $x_i$  and the temporal grids defined by  $t^n$  upon which the numerical solutions  
 55    are calculated. Firstly these grids are uniform so that  $\Delta x = x_i - x_{i-1} \forall i$  and  $\Delta t =$   
 56     $t^n - t^{n-1} \forall n$  are both constant. Secondly subscripts and superscripts are used to denote  
 57    where a quantity  $q$  is evaluated in the following way  $q_i^n = q(x_i, t^n)$ . Lastly a cell is a  
 58    particularly useful unit of the finite volume method, where the  $i$ th cell is the interval  
 59     $[x_i - \Delta x/2, x_i + \Delta x/2]$  centred around  $x_i$ .

60    2.1.1. Distance between Numerical Results

61    By measuring the relative distance between numerical solutions we can assess  
 62    whether our numerical solutions are converging as  $\Delta x \rightarrow 0$ . Rather than comparing  
 63    all numerical results to one another all numerical solutions are compared to the one  
 64    with the smallest  $\Delta x$ . In these experiments  $\Delta x$  was lowered by dividing it by 2 thus the  
 65    grid built from the smallest  $\Delta x$  contains all the locations  $x_i$  in the grid built from the  
 66    larger  $\Delta x$  values. To measure the relative distance between quantities on these grids we  
 67    compare them only on the common points  $x_i$  in the larger  $\Delta x$  grid. So that for some  
 68    quantity  $q$  we have our numerical approximation to it on the grid built from the smallest  
 69     $\Delta x$   $q^*$  and on the grid built from the grid larger  $\Delta x$   $q'$  with the relative distance between  
 70    the two being

$$71 \quad L_1^q = \frac{\sum_i |q'(x_i) - q^*(x_i)|}{\sum_i |q^*(x_i)|}. \quad (4)$$

73    2.1.2. Conserved Quantities

74    The initial conditions of the smoothed dam-break (3) were integrated to get the  
 75    following expressions for  $C_h(0)$ ,  $C_{uh}(0)$  and  $C_H(0)$  provided  $x_0$  is the midpoint of the  
 76    spatial domain  $[a, b]$  in which the smoothed dam-break occurs

$$77 \quad C_h(0) = \frac{h_1 + h_0}{2} (b - a),$$

$$80 \quad C_{uh}(0) = 0$$

82 and

$$83 \quad C_{\mathcal{H}}(0) = \frac{g}{4} \left( h_0^2 - h_1^2 + \alpha (h_1 - h_0)^2 \tanh \left( \frac{a-b}{2\alpha} \right) \right).$$

85

86 To calculate the total amount of a quantity  $q$  in our numerical solution we fit a  
 87 quartic interpolant of the primitive variables  $h$  and  $u$  over a cell utilising quantities  
 88 from neighbouring cells and then apply Gaussian quadrature with 3 points to get a  
 89 good approximation to the total amount of  $q$  in a cell. The amounts of  $q$  in each cell  
 90 are summed across all cells to get the total amount of  $q$  in the domain at time  $t$  which  
 91 we call  $C^*_q(t)$ . The error in conservation of a quantity  $q$  for a numerical method is

$$92 \quad C_1^q = \frac{|C_q(0) - C^*_q(t)|}{|C_q(0)|}. \quad (6)$$

93 Note that for  $uh$  the denominator is 0 and that there is a flux of momentum due to the  
 94 unequal heights at both ends of the domain. To resolve these issues for  $uh$  the error in  
 95 the conservation of  $uh$  is measured by  
 96

$$97 \quad C_1^{uh} = \left| C_{uh}(0) - C^*_{uh}(t) - \frac{gt}{2} (h(b)^2 - h(a)^2) \right|. \quad (7)$$

### 99 2.1.3. Whitham Modulation for Undular Bores of the Serre Equations

100 Undular bores for the one dimensional Serre equations were analysed by El et al.  
 101 [1] and an expression for the amplitude ( $A^+$ ) of the leading wave of an undular bore  
 102 shown in Figure 3 was given

$$103 \quad \frac{\Delta}{(A^+ + 1)^{1/4}} - \left( \frac{3}{4 - \sqrt{A^+ + 1}} \right)^{21/10} \left( \frac{2}{1 + \sqrt{A^+ + 1}} \right)^{2/5} = 0 \quad (8)$$

104 where  $\Delta = h_b/h_0$ , and  $h_b$  is the amplitude of the bore. The height of the bore created  
 105 by the dam-break in (8) used by El et al. [1] was

$$h_b = \frac{1}{4} \left( \sqrt{\frac{h_1}{h_0}} + 1 \right)^2.$$

106 Thus for our dam-break problem  $h_b = 1.37082$  m,  $\Delta = 1.37082$  and  $A^+ = 1.73998$  m.

### 107 2.2. Shallow Water Wave Equation Analytic Solution

108 Le Métayer et al. [2] and Mitsotakis et al. [3] demonstrated that the analytic solution  
 109 of the shallow water wave equations for the dam-break problem captures the mean  
 110 behaviour of their numerical results for the Serre equations. In section 4 the validity of  
 111 this comparison is assessed and so the relevant background required for it is presented  
 112 here.

113 For the discontinuous dam-break problem the shallow water wave equations, which  
 114 are the Serre equations with dispersive terms neglected, can be solved analytically. The  
 115 analytic solution of the shallow water wave equations has been used as a comparative

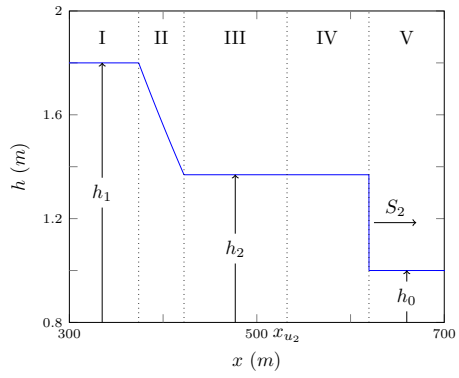


Figure 2: Analytic solution at  $t = 30\text{s}$  of the shallow water wave equations for the dam-break problem with  $h_0 = 1\text{m}$ ,  $h_1 = 1.8\text{m}$  and  $x_0 = 100\text{m}$ .

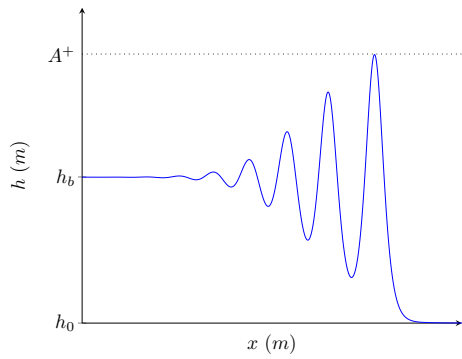


Figure 3: Demonstration of quantities obtained by Whitham modulation for undular bores of the Serre equations.

115 tool against numerical results in the literature [2, 3] as they appear to capture the mean  
 116 behaviour of the numerical solutions.

117 An example of the analytic solution of the shallow water wave equations for the  
 118 dam-break problem is presented in Figure 2 at  $t = 30s$ . Region I is the undisturbed  
 119 water upstream of the dam-break at constant height ( $h_1$ ) and velocity (0m/s) and region  
 120 II is the rarefaction fan connecting regions I and III. Regions III and IV are the constant  
 121 height ( $h_2$ ) and constant velocity ( $u_2$ ) state which are separated by  $x_{u_2} = x_0 + u_2 t$  and  
 122 region V is the undisturbed water downstream at constant height ( $h_0$ ) and velocity  
 123 (0m/s) separated from region IV by a shock which travels at velocity  $S_2$ . Expressions  
 124 for the unknown quantities  $h_2$ ,  $u_2$  and  $S_2$  in terms of  $h_0$  and  $h_1$  were given by Wu et al.  
 125 [11]

$$126 \quad h_2 = \frac{h_0}{2} \left( \sqrt{1 + 8 \left( \frac{2h_2}{h_2 - h_0} \frac{\sqrt{gh_1} - \sqrt{gh_2}}{\sqrt{gh_0}} \right)^2} - 1 \right), \quad (9a)$$

127

$$129 \quad u_2 = 2 \left( \sqrt{gh_1} - \sqrt{gh_2} \right) \quad (9b)$$

130 and

$$132 \quad S_2 = \frac{h_2 u_2}{h_2 - h_0}. \quad (9c)$$

134 Applying (9) to our dam-break problem heights results in  $h_2 = 1.36898m$  ,  $u_2 =$   
 135  $1.074975 m/s$  and  $S_2 = 3.98835 m/s$  which are demonstrated in Figure 2.

### 136 3. Numerical Methods

137 Five numerical schemes are used to solve the Serre equations. The first ( $\mathcal{V}_1$ ), sec-  
 138 ond ( $\mathcal{V}_2$ ) and third-order ( $\mathcal{V}_3$ ) methods of [5], the method of El et al. [1] ( $\mathcal{E}$ ) and a  
 139 second-order finite difference method ( $\mathcal{G}$ ).

140 The  $\mathcal{V}_i$  methods are stable under the CFL condition [12] and have demonstrated  
 141 the appropriate order of convergence for smooth problems [5]. Furthermore,  $\mathcal{V}_2$  and  
 142  $\mathcal{V}_3$  have been validated against experimental data containing steep gradients [5]. The  
 143 two methods  $\mathcal{G}$  and  $\mathcal{E}$  were found to be stable under the CFL condition as well, and for  
 144 completeness these methods are presented in the Appendix to allow for replication.

145 Generally we find that  $\mathcal{V}_1$  is the worst performing of these methods due to its diffu-  
 146 sivity [5]. Of the high-order methods  $\mathcal{E}$  is the worst performing, introducing dispersive  
 147 errors. The methods  $\mathcal{V}_2$  and  $\mathcal{V}_3$  produce very similar numerical solutions [5], while  
 148 the numerical solutions of  $\mathcal{G}$  are also close to them.

### 149 4. Numerical Results

150 We begin by looking into the effect of the initial steepness of the smoothed dam-  
 151 break problem for different  $\alpha$  values by observing what happens as  $\Delta x \rightarrow 0$  and our  
 152 numerical solutions better approximate the true solution of the Serre equations. We

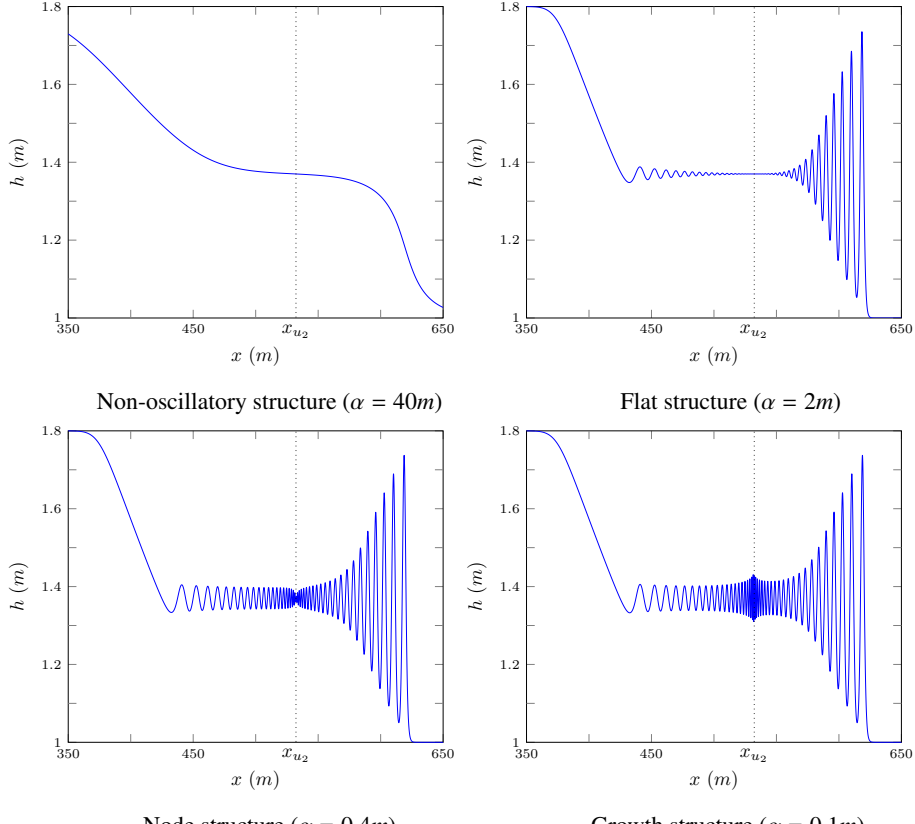


Figure 4: Numerical results of  $\mathcal{V}_3$  with  $\Delta x = 10/2^{11}m$  (—) at  $t = 30s$  for various smooth dam-break problems demonstrating the different observed structures.

then investigate numerical results for long time scales and how the shallow water wave equations analytic solution compare to our numerical solutions.

All numerical methods used  $\Delta t = 0.01\Delta x$  which is smaller than required by the CFL condition [12] which ensures stability of our schemes. The time step  $\Delta t$  was chosen to be smaller than necessary because for a final time of  $t = 30s$  making  $\Delta t$  small suppresses errors without excessively increasing the run-time of the experiments. The method  $\mathcal{V}_2$  requires an input parameter to its slope limiter and this was chosen to be  $\theta = 1.2$  [5]. All of the numerical methods presented use Dirichlet boundary conditions with  $u = 0m/s$  at both boundaries and  $h = 1.8m$  on the left and  $h = 1m$  on the right.

#### 4.1. Observed Structures of the Numerical Solutions

We observe that there are four different structures as  $\Delta x \rightarrow 0$  depending on the  $\alpha$  and the numerical method. They are the non-oscillatory structure, the flat structure, the node structure and the growth structure. An example of each of these structures is in Figure 4 for  $\mathcal{V}_3$ 's numerical solutions to various smoothed dam-break problems.

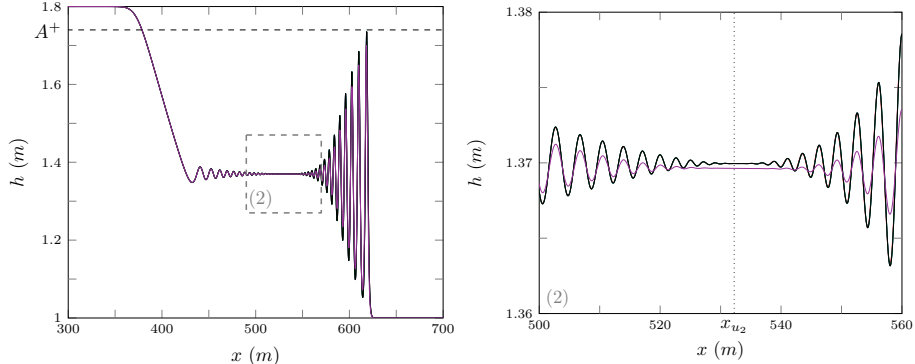


Figure 5: Numerical solutions  $\mathcal{G}$  (blue),  $\mathcal{E}$  (red),  $\mathcal{V}_3$  (green),  $\mathcal{V}_2$  (black) and  $\mathcal{V}_1$  (purple) with  $\Delta x = 10/2^{11}m$  at  $t = 30s$  for the smooth dam-break problem with  $\alpha = 2m$ .

167     The four structures are identified by the nature of the numerical solutions in regions  
 168     III and IV when  $\Delta x$  is small and they correspond to different structures in the numerical  
 169     solutions presented in the literature. From Figure 4 it can be seen that as  $\alpha$  is decreased,  
 170     steepening the initial conditions the numerical solutions demonstrate an increase in the  
 171     size and number of oscillations particularly around  $x_{u2}$ .

172     For the non-oscillatory and flat structures there is excellent agreement between all  
 173     higher-order numerical methods at our highest resolution  $\Delta x = 10/2^{11}m$ . An illus-  
 174     tration of this agreement is given in Figure 5 for the flat structure which is the most  
 175     difficult to resolve of the two structures. Since the first-order scheme is diffusive [5]  
 176     we find that although it's highest resolution numerical solution has the same behaviour  
 177     as the other methods it damps the oscillations.

178     *4.1.1. Non-oscillatory Structure*

179     The first structure is the non-oscillatory structure it is the result of a large  $\alpha$ . When  
 180      $\alpha$  is large for the smoothed dam-break problem the fluid to the left of  $x_0$  flows to fill the  
 181     right side, but due to the large  $\alpha$  the front of this flow is not steep enough to generate  
 182     undulations over short time spans. Eventually the front of this flow steepens due to  
 183     non-linearity and undulations develop there.

184     This structure is not present in the literature as no authors chose large enough  $\alpha$ . An  
 185     example of this structure can be seen in Figure 6 for  $\alpha = 40m$  using  $\mathcal{V}_3$ . Because this  
 186     is a very smooth problem we observe that all numerical results are visually identical  
 187     for all  $\Delta x < 10/2^4m$ .

188     From Table 1 it can be seen that not only have these solutions converged visually but  
 189     the  $L_1$  measures demonstrate that we have reached convergence to round-off error by  
 190      $\Delta x = 10/2^8m$  after which the relative difference between numerical solutions plateau.

191     Table 1 also demonstrates that the error in conservation of the numerical solutions  
 192     are at round-off error for  $h$  and  $\mathcal{H}$ .  $C_1^{uh}$  is the worst performing of the measures because  
 193     the smoothed dam-break has such a large  $\alpha$  that  $h(0m) \neq 1.8m$  and  $h(1000m) \neq 1m$   
 194     causing unequal fluxes in momentum at the boundaries.

195     Because the initial conditions are not steep enough an undular bore has not devel-  
 196     oped by  $t = 30s$  thus the Whitham modulation results for leading wave amplitude do

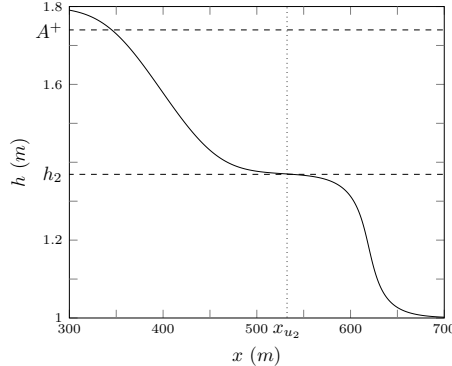


Figure 6: Numerical results of  $\mathcal{V}_3$  at  $t = 30s$  for smooth dam-break problem with  $\alpha = 40m$  for  $\Delta x = 10/2^{10}m$  (—),  $10/2^8m$  (—),  $10/2^6m$  (—) and  $10/2^4m$  (—).

not apply.

The convergence and conservation of numerical solutions as  $\Delta x \rightarrow 0$  together with the agreement of different numerical methods demonstrates that the numerical result in Figure 6 and its non-oscillatory structure is an accurate representation of the solutions of the Serre equations when  $\alpha$  is sufficiently large and in particular  $\alpha = 40m$ .

#### 4.1.2. Flat Structure

The second structure will be referred to as the flat structure due to the presence of a constant height around  $x_{u2}$ , this is the most common structure observed in the literature [2, 3, 4]. It is generated as are the rest of the structures when the initial conditions are steep enough such that the bore that develops has undulations. This structure consists of oscillations in regions III and IV which are separated by a constant height state around  $x_{u2}$ . An example of the structure can be seen in the numerical solutions presented in Figure 7 when  $\alpha = 2m$ .

As  $\Delta x$  decreases the numerical solutions converge so that by  $\Delta x = 10/2^8m$  the solutions for higher  $\Delta x$  are visually identical. Table 1 demonstrates that although we have convergence visually the  $L_1$  measures are still decreasing and haven't plateaued. Likewise the  $C_1$  are still decreasing and have only reached round-off error for  $h$ , although our numerical solutions are close to one another and exhibit good conservation. This indicates that to precisely resolve the numerical solutions for  $\mathcal{V}_3$  of this smoothed dam-break problem down to round-off error would require an even lower  $\Delta x$ .

Figures 7 and 5 demonstrate good agreement between the numerical solutions and  $A^+$  derived from the Whitham modulation of El et al. [1].

The convergence of our numerical solutions as  $\Delta x \rightarrow 0$  of  $\mathcal{V}_3$  both in Figure 7 and Table 1, the agreement of all the models in Figure 5 with  $\Delta x = 10/2^{11}m$  and agreement of the numerical solutions and  $A^+$  demonstrates that while our solutions have not converged down to round-off error our numerical solutions are accurate approximate solutions of the Serre equations for the smoothed dam-break problem with  $\alpha = 0.5m$ .

These numerical solutions compare well with those of Mitsotakis et al. [3] who use the same  $\alpha$  but different  $h_0$  and  $h_1$  and resolve the same behaviour. We found that we resolved this structure for all methods at  $\Delta x = 10/2^{11}m$  for the smoothed dam-break

$\alpha$	$\Delta x$	$C_1^h$	$C_1^{uh}$	$C_1^H$	$L_1^h$	$L_1^u$
40	$10/2^4$	$12 \cdot 10^{-11}$	$1.77 \cdot 10^{-6}$	$1.23 \cdot 10^{-8}$	$1.74 \cdot 10^{-7}$	$2.90 \cdot 10^{-6}$
40	$10/2^6$	$1.07 \cdot 10^{-11}$	$1.50 \cdot 10^{-6}$	$1.49 \cdot 10^{-10}$	$2.57 \cdot 10^{-9}$	$4.19 \cdot 10^{-8}$
40	$10/2^8$	$8.77 \cdot 10^{-13}$	$5.49 \cdot 10^{-7}$	$3.77 \cdot 10^{-13}$	$6.08 \cdot 10^{-11}$	$5.28 \cdot 10^{-10}$
40	$10/2^{10}$	$1.77 \cdot 10^{-11}$	$2.21 \cdot 10^{-8}$	$3.56 \cdot 10^{-11}$	$2.54 \cdot 10^{-11}$	$6.49 \cdot 10^{-11}$
2	$10/2^4$	$4.9 \cdot 10^{-14}$	$5.10 \cdot 10^{-3}$	$8.69 \cdot 10^{-4}$	$5.02 \cdot 10^{-3}$	$6.77 \cdot 10^{-2}$
2	$10/2^6$	$2.51 \cdot 10^{-13}$	$2.18 \cdot 10^{-4}$	$6.58 \cdot 10^{-5}$	$4.14 \cdot 10^{-4}$	$5.20 \cdot 10^{-3}$
2	$10/2^8$	$9.81 \cdot 10^{-13}$	$7.72 \cdot 10^{-7}$	$5.01 \cdot 10^{-7}$	$6.00 \cdot 10^{-6}$	$7.59 \cdot 10^{-5}$
2	$10/2^{10}$	$3.95 \cdot 10^{-12}$	$5.56 \cdot 10^{-9}$	$6.13 \cdot 10^{-9}$	$1.76 \cdot 10^{-7}$	$2.33 \cdot 10^{-6}$
0.4	$10/2^4$	$9 \cdot 10^{-14}$	$4.82 \cdot 10^{-3}$	$1.02 \cdot 10^{-3}$	$6.79 \cdot 10^{-3} \dagger$	$9.93 \cdot 10^{-2} \dagger$
0.4	$10/2^6$	$2.4 \cdot 10^{-13}$	$2.41 \cdot 10^{-4}$	$1.11 \cdot 10^{-4}$	$8.89 \cdot 10^{-4} \dagger$	$1.13 \cdot 10^{-2} \dagger$
0.4	$10/2^8$	$9.68 \cdot 10^{-13}$	$7.57 \cdot 10^{-7}$	$2.25 \cdot 10^{-6}$	$1.53 \cdot 10^{-5} \dagger$	$1.91 \cdot 10^{-4} \dagger$
0.4	$10/2^{10}$	$3.91 \cdot 10^{-12}$	$4.95 \cdot 10^{-9}$	$2.01 \cdot 10^{-8}$	$3.61 \cdot 10^{-7} \dagger$	$5.00 \cdot 10^{-6} \dagger$
0.1	$10/2^4$	$7.6 \cdot 10^{-14}$	$4.82 \cdot 10^{-3}$	$1.06 \cdot 10^{-3}$	$7.04 \cdot 10^{-3} \dagger$	$1.02 \cdot 10^{-1} \dagger$
0.1	$10/2^6$	$2.4 \cdot 10^{-13}$	$2.39 \cdot 10^{-4}$	$1.44 \cdot 10^{-4}$	$1.02 \cdot 10^{-3} \dagger$	$1.28 \cdot 10^{-2} \dagger$
0.1	$10/2^8$	$9.79 \cdot 10^{-13}$	$2.21 \cdot 10^{-7}$	$1.20 \cdot 10^{-5}$	$2.86 \cdot 10^{-5} \dagger$	$3.46 \cdot 10^{-4} \dagger$
0.1	$10/2^{10}$	$3.92 \cdot 10^{-12}$	$4.46 \cdot 10^{-8}$	$7.61 \cdot 10^{-7}$	$4.99 \cdot 10^{-7} \dagger$	$6.40 \cdot 10^{-6} \dagger$

Table 1: All errors in conservation  $C_1^q$  for the conserved quantities and relative distances  $L_1^q$  of the primitive variables for numerical solutions of  $\mathcal{V}_3$ .  $L_1^q$  uses the numerical solution with  $\Delta x = 10/2^{11}m$  as the high resolution basis of comparison and  $\dagger$  indicates the omission of the interval  $[520m, 540m]$  from the comparison.

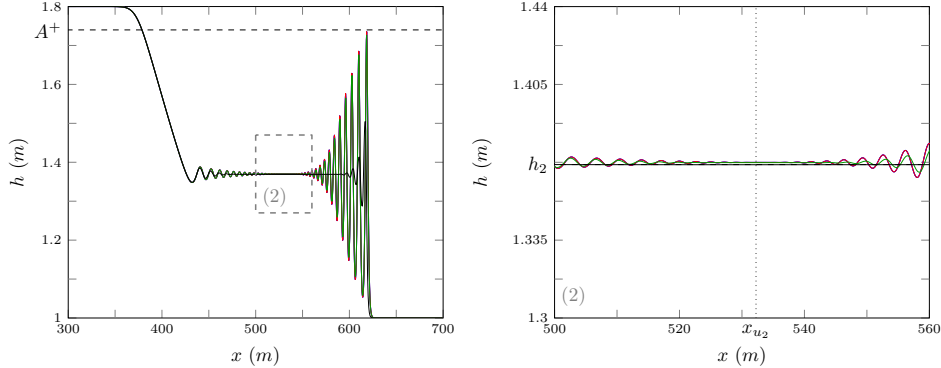


Figure 7: Numerical results of  $\mathcal{V}_3$  at  $t = 30s$  for the smooth dam-break problem with  $\alpha = 2m$  for  $\Delta x = 10/2^{10}m$  (blue),  $10/2^8m$  (red),  $10/2^6m$  (green) and  $10/2^4m$  (black).

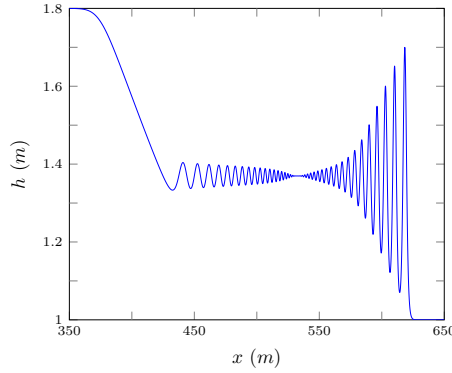


Figure 8: Numerical solution of  $\mathcal{V}_1$  at  $t = 30s$  for the smooth dam-break problem with  $\alpha = 0.001m$  for  $\Delta x = 10/2^{11}m$  (blue).

with  $\alpha$ 's as low as  $1m$ . This is the same behaviour that is present in the numerical solutions of Mitsotakis et al. [4] who use  $\alpha = 1m$  but different heights. Therefore Mitsotakis et al. [3] and Mitsotakis et al. [4] only observe the flat scenario in their numerical results due to their choice of  $\alpha$  for the smoothed dam-break problem.

The first-order  $\mathcal{V}_1$  is diffusive [5] and damps oscillations that are present in higher-order methods numerical results as in Figure 5. We find that for any  $\alpha \leq 4m$  and the discontinuous dam-break problem our numerical solutions of  $\mathcal{V}_1$  at  $t = 30s$  with  $\Delta x = 10/2^{11}m$  can only resolve the flat scenario which can be seen in Figure 8 for  $\alpha = 0.001m$ . Therefore Le Métayer et al. [2] using  $\mathcal{V}_1$  with their chosen  $\Delta x$  and  $\Delta t$  which are larger than our  $\Delta x$  and  $\Delta t$  could only resolve the flat structure.

#### 4.1.3. Node Structure

The third structure will be referred to as the node structure and it was observed by El et al. [1]. The node structures main feature is that the oscillations in region III and IV decay and appear to meet at  $x_{u_2}$  as can be seen in Figure 9 when  $\alpha = 0.4m$ .

Figure 9 demonstrates that our numerical solutions have not converged, however

242 this is only in the area around  $x_{u_2}$ . Due to the large difference in numerical solutions  
243 around  $x_{u_2}$  the  $L_1$  measure over the area around  $x_{u_2}$  would not be insightful, however by  
244 omitting this region we can gain some knowledge about how well our solutions agree  
245 away from  $x_{u_2}$ . This was performed for the relevant  $L_1$  measures in Table 1 by omitting  
246 the interval  $[520m, 540m]$ . These modified  $L_1$  measures demonstrate that while our  
247 numerical results have visually converged away from  $x_{u_2}$  they have not fully converged  
248 down to round-off error under the  $L_1$  measure although they are close to one another  
249 away from  $x_{u_2}$ .

250 Table 1 demonstrates that the  $C_1$  measures are decreasing as well and have only  
251 reached round-off error for  $h$ . Therefore to resolve the converged numerical solution  
252 of this particular smoothed dam-break problem down would require even lower  $\Delta x$   
253 values.

254 There is a good agreement across different numerical methods for  $\Delta x = 10/2^{11}m$   
255 as can be seen in Figure 10. In particular all the higher-order methods exhibit the  
256 same behaviour and most only disagree in a very small region around  $x_{u_2}$ , although  
257 we observe that  $\mathcal{E}$  has not converged as well to the numerical solutions of the other  
258 methods.

259 Figures 9 and 10 demonstrate good agreement between the numerical solutions and  
260  $A^+$  derived from Whitham modulation across different methods and different  $\Delta x$ .

261 The behaviour of  $\mathcal{V}_3$ 's solutions as  $\Delta x \rightarrow 0$ , the agreement of different numerical  
262 methods when  $\Delta x = 10/2^{11}m$  and the agreement of our numerical solutions with  
263  $A^+$  demonstrates that while our numerical solutions have not completely visually con-  
264 verged they are an accurate representation of the solutions of the Serre equations for  
265 the smoothed dam-break problem with  $\alpha = 0.4m$ . In particular for  $\alpha = 0.4m$  the node  
266 structure should be observed in numerical solutions of the Serre equations.

267 These numerical solutions support the findings of El et al. [1] who also use some  
268 smoothing [13] but do not report what smoothing was performed. Using their method  
269  $\mathcal{E}$  and similar  $\Delta x$  to El et al. [1] we are able to resolve the growth behaviour for smaller  
270  $\alpha$ 's, indicating that the smoothing performed by El et al. [1] limited their observed  
271 behaviour to just the node structure.

#### 272 4.1.4. Growth Structure

273 The fourth structure is the growth structure which has hitherto not been published.  
274 It features a growth in the oscillation amplitude around  $x_{u_2}$ . An example of the growth  
275 structure can be seen for  $\mathcal{V}_3$ 's numerical solutions in Figure 11 of the smoothed dam-  
276 break problem with  $\alpha = 0.1m$ . This structure was observed in the numerical solutions  
277 of  $\mathcal{V}_3$  for  $\Delta x = 10/2^{11}m$  at  $t = 30s$  for  $\alpha$ 's as low as  $0.001m$  and even for the discon-  
278 tinuous dam-break problem.

279 Figure 11 shows that this behaviour can only be observed for  $\Delta x = 10/2^{10}m$ , with  
280 poor convergence of the numerical results around  $x_{u_2}$ . Again our  $L_1$  measures in Table 1  
281 omit the interval  $[520m, 540m]$  to compare the numerical solutions. This demonstrates  
282 that away from  $x_{u_2}$  our numerical solutions are quite close to one another but they have  
283 not converged to round-off error as  $\Delta x \rightarrow 0$ . The  $C_1$  measures in Table 1 are still  
284 decreasing and have only attained round-off error for  $h$ , although for  $uh$  and  $\mathcal{H}$  the  
285 errors in conservation are still small. These measures continue the trend in Table 1

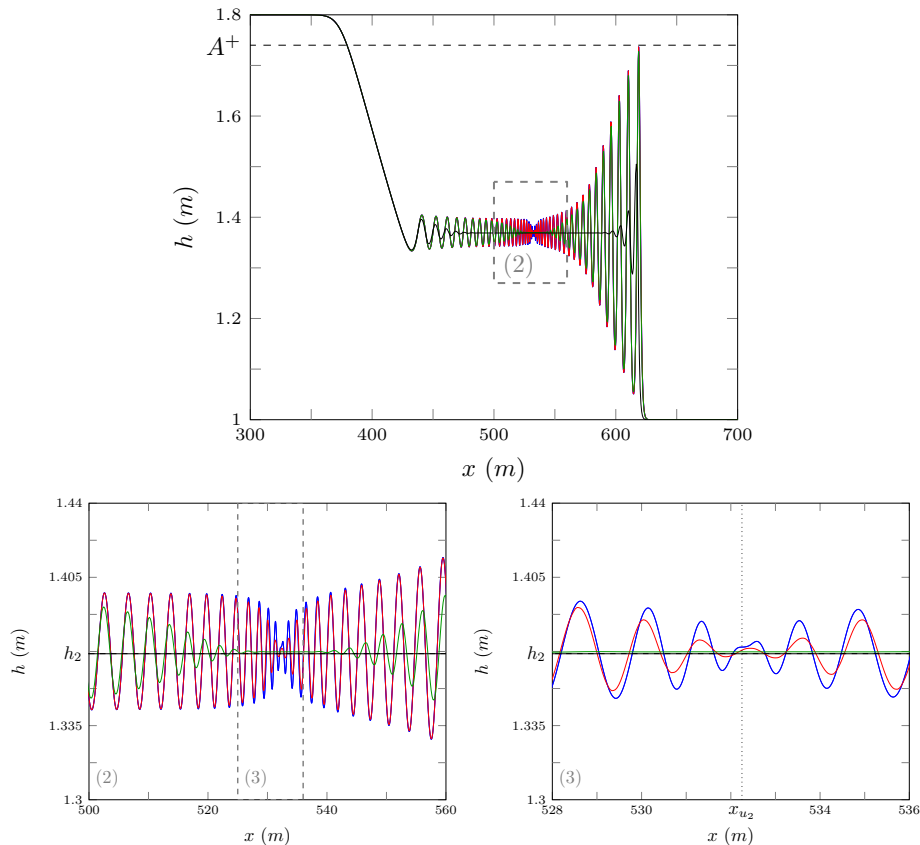


Figure 9: Numerical solution of  $\mathcal{V}_3$  at  $t = 30s$  for the smooth dam-break problem with  $\alpha = 0.4m$  for  $\Delta x = 10/2^{10}m$  (blue),  $10/2^8m$  (red),  $10/2^6m$  (green) and  $10/2^4m$  (black).

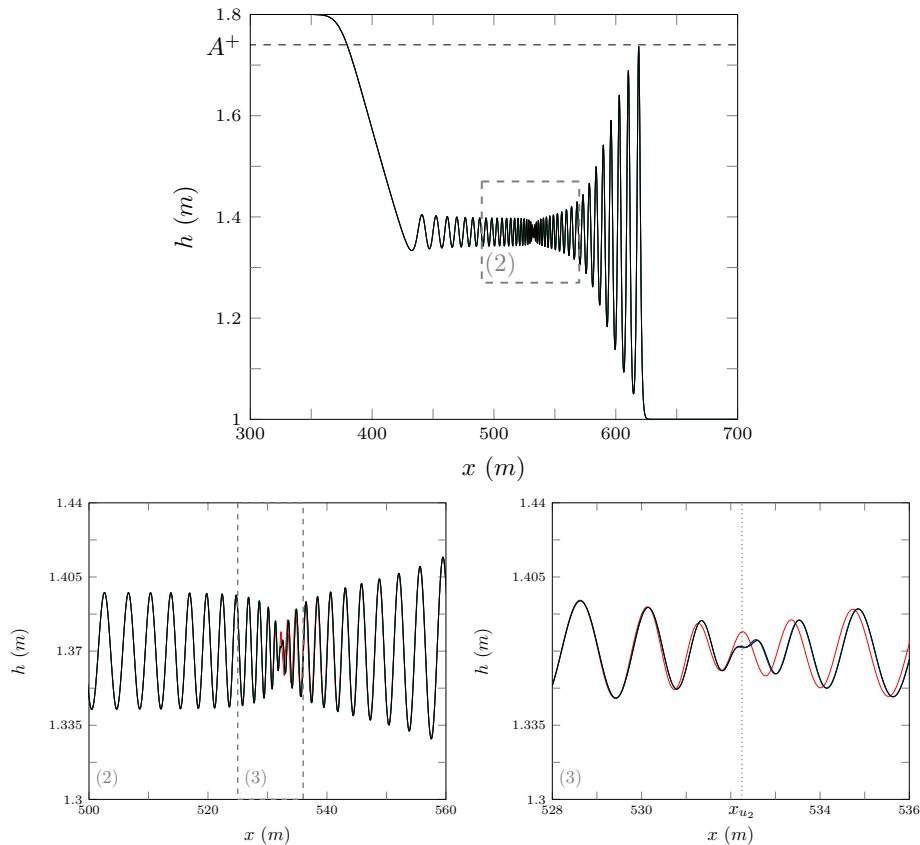


Figure 10: Numerical solution of  $\mathcal{G}$  (blue),  $\mathcal{E}$  (red),  $\mathcal{V}_3$  (green) and  $\mathcal{V}_2$  (black) at  $t = 30s$  with  $\Delta x = 10/2^{11}m$  for the smoothed dam-break problem with  $\alpha = 0.4m$ .

286 where smaller  $\alpha$ 's and thus steeper initial conditions lead to poorer convergence and  
287 conservation because they are more difficult to solve accurately.

288 Figures 11 and 12 demonstrate good agreement between the numerical solutions  
289 and  $A^+$  derived from Whitham modulation.

290 Figure 12 demonstrates that our numerical solutions for  $\Delta x = 10/2^{11}m$  with the  
291 best methods  $\mathcal{E}$ ,  $\mathcal{V}_3$  and  $\mathcal{V}_2$  disagree for only a few oscillations around  $x_{u_2}$ . Since both  
292  $\mathcal{G}$  and  $\mathcal{E}$  are second-order finite difference methods their errors are dispersive meaning  
293 that oscillation size and number in their numerical solutions are overestimated, as can  
294 be seen for the large dispersive errors of  $\mathcal{E}$ . All  $\mathcal{V}_i$  methods are diffusive and therefore  
295 underestimate the size and number of oscillations in their numerical solutions. Therefore  
296 the true solution of the Serre equations should be between the dispersive method  
297  $\mathcal{G}$  and the diffusive method  $\mathcal{V}_3$  which is a growth structure.

298 These results indicate that the solutions of the Serre equations to the smoothed  
299 dam-break with sufficiently small  $\alpha$ 's should exhibit a growth structure at  $t = 30s$ , even  
300 though we have not precisely resolved all the oscillations in our numerical solutions.

301 It was found that decreasing  $\alpha$  did increase the amplitude of the oscillations around  
302  $x_{u_2}$  but not drastically, for  $\mathcal{V}_3$  with  $\Delta x = 10/2^{11}m$  and  $\alpha = 0.001m$  the oscillations in  $h$   
303 were bounded by the interval  $[1.28m, 1.46m]$ . Of particular note is that the number of  
304 oscillations are the same in Figures 10 and 12 for the best methods even though they  
305 have different structures.

#### 306 4.2. Shallow water wave equation comparison

307 The analytic solutions of shallow water wave equations have been used as a guide  
308 for the mean behaviour of the solution of the Serre equations for the dam-break problem  
309 in the literature [2, 3].

310 To assess the applicability of this the mean of our numerical solution of  $u$  and  $h$  in  
311 the interval  $[x_{u_2} - 50m, x_{u_2} + 50m]$  were calculated for a range of different smoothed  
312 dam-break height ratios and compared to their respective approximation from the shal-  
313 low water wave equations  $u_2$  and  $h_2$ . The results of this can be seen in Figure 13 for  
314 numerical solutions of  $\mathcal{V}_3$  where  $\Delta x = 10/2^{10}m$  for the smoothed dam-break with  
315  $\alpha = 0.1m$  at  $t = 100s$  where  $h_0$  is fixed and  $h_1$  is varied. It can be seen that although  
316 these results are not precise the values  $h_2$  and  $u_2$  are good approximations to the mean  
317 behaviour of the fluid inside the bore for a range of different aspect ratios.

#### 318 5. Conclusions

319 Utilising two finite difference methods of second-order and three finite difference-  
320 volume hybrid methods of various orders an investigation into the smoothed dam-break  
321 problem with varying steepness was performed. Four different structures of the numer-  
322 ical solutions were uncovered and demonstrated to be valid, the general trend of these  
323 structures is that an increase in steepness increases the size and number of oscillations  
324 in the solution. This study explains the different structures exhibited by the numerical  
325 results in the literature for the solution of the smoothed dam-break problem for Serre  
326 equations and uncovers a new result. We find that the analytic solution of the shallow  
327 water wave equations for the dam-break problem is a good guide to the mean behaviour  
328 of the Serre equations for the smoothed dam-break problem with various aspect ratios.

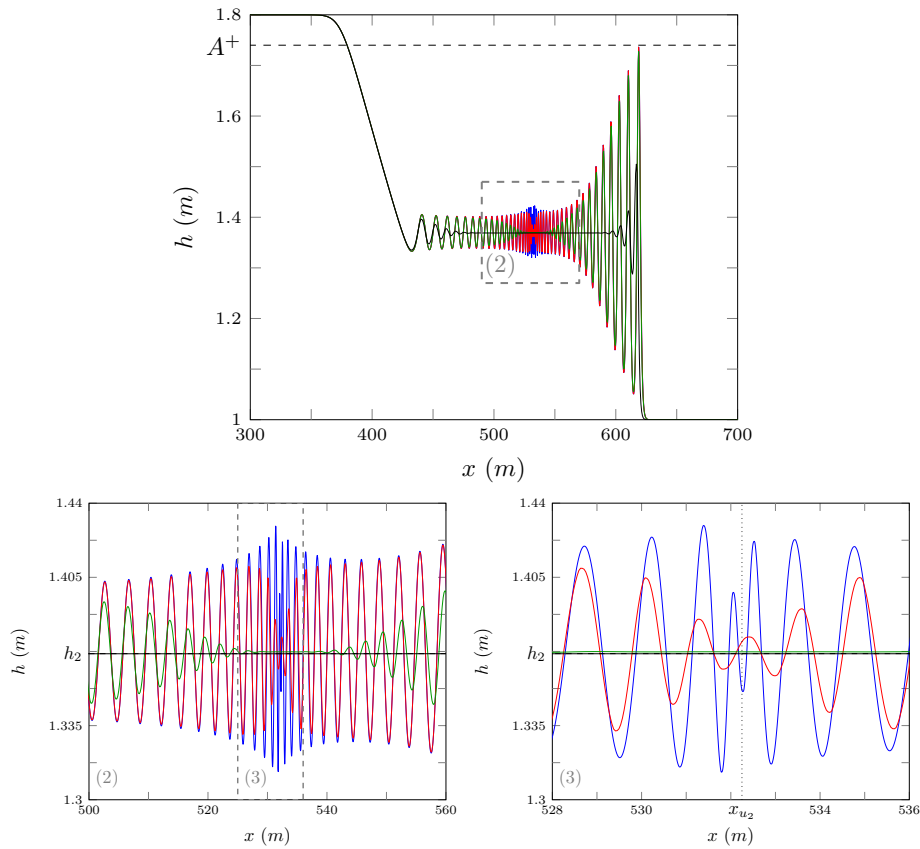


Figure 11: Numerical solutions of  $\mathcal{V}_3$  at  $t = 30s$  for the smooth dam-break problem with  $\alpha = 0.1m$  for  $\Delta x = 10/2^{10}m$  (blue),  $10/2^8m$  (red),  $10/2^6m$  (green) and  $10/2^4m$  (black).

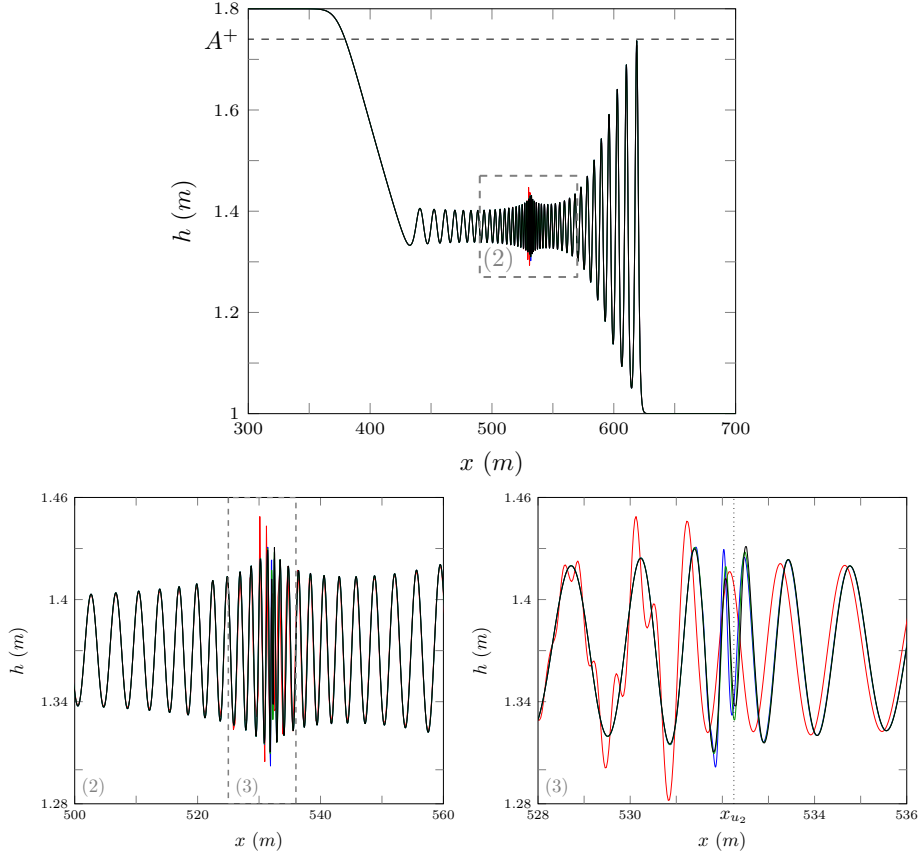


Figure 12: Numerical solutions of  $\mathcal{G}$  (blue dashed),  $\mathcal{E}$  (red solid),  $\mathcal{V}_3$  (green solid) and  $\mathcal{V}_2$  (black solid) at  $t = 30s$  with  $\Delta x = 10/2^{11}m$  for the smoothed dam-break problem with  $\alpha = 0.1m$ .

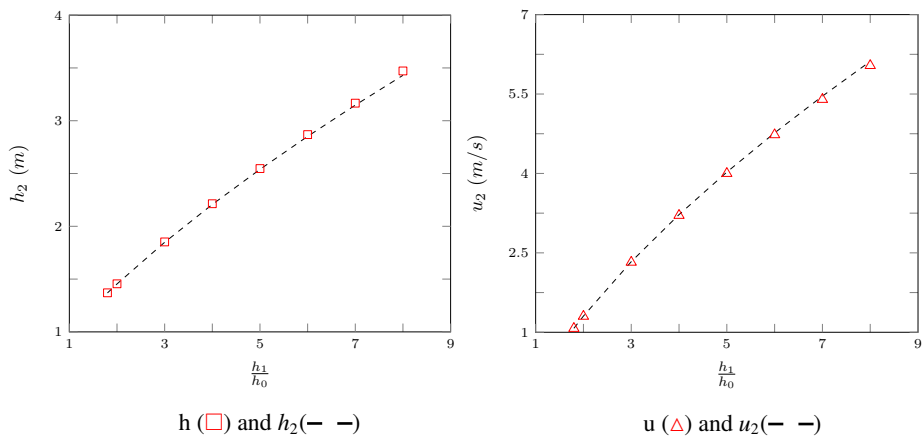


Figure 13: Comparison between mean behaviour of the Serre equations and the values of the analytic solution of the shallow water wave equations that approximate them for a range of different aspect ratios.

- 329 [1] G. El, R. H. J. Grimshaw, N. F. Smyth, Unsteady undular bores in fully nonlinear  
 330 shallow-water theory, *Physics of Fluids* 18 (027104).
- 331 [2] O. Le Métayer, S. Gavrilyuk, S. Hank, A numerical scheme for the GreenNaghdi  
 332 model, *Journal of Computational Physics* 229 (6) (2010) 2034–2045.
- 333 [3] D. Mitsotakis, B. Ilan, D. Dutykh, On the Galerkin/Finite-Element Method for  
 334 the Serre Equations, *Journal of Scientific Computing* 61 (1) (2014) 166–195.
- 335 [4] D. Mitsotakis, D. Dutykh, J. Carter, On the nonlinear dynamics of the traveling-  
 336 wave solutions of the Serre system, *Wave Motion* 70 (1) (2017) 166–182.
- 337 [5] C. Zoppou, J. Pitt, S. Roberts, Numerical Solution of the Fully Non-linear Weakly  
 338 Dispersive Serre Equations for Steep Gradient Flows, *Applied Mathematical  
 339 Modelling* 00 (00) (2017) 00–00.
- 340 [6] C. H. Su, C. S. Gardner, Korteweg-de Vries equation and generalisations. III.  
 341 Derivation of the Korteweg-de Vries equation and Burgers equation, *Journal of  
 342 Mathematical Physics* 10 (3) (1969) 536–539.
- 343 [7] D. Lannes, P. Bonneton, Derivation of asymptotic two-dimensional time-  
 344 dependent equations for surface water wave propagation, *Physics of Fluids* 21 (1)  
 345 (2009) 16601–16610.
- 346 [8] M. Li, P. Guyenne, F. Li, L. Xu, High order well-balanced CDG-FE methods  
 347 for shallow water waves by a Green-Naghdi model, *Journal of Computational  
 348 Physics* 257 (2014) 169–192.
- 349 [9] Y. A. Li, Hamiltonian Structure and Linear Stability of Solitary Waves of the  
 350 Green-Naghdi Equations, *Journal of Nonlinear Mathematical Physics* 9 (2002)  
 351 99–105.
- 352 [10] A. E. Green, P. M. Naghdi, A derivation of equations for wave propagation in  
 353 water of variable depth, *Journal of Fluid Mechanics* 78 (2) (1976) 237–246.
- 354 [11] C. Wu, G. Huang, Y. Zheng, Theoretical solution of dam-break shock wave, *Jour-  
 355 nal of Hydraulic Engineering* 125 (11) (1999) 1210–1215.
- 356 [12] A. A. Harten, High resolution schemes for hyperbolic conservation laws, *Journal  
 357 of Computational Physics* 49 (3) (1983) 357–393.
- 358 [13] G. El, M. Hoefer, Dispersive shock waves and modulation theory, *Physica D:  
 359 Nonlinear Phenomena* 333 (2016) 11–65.

360 **Appendix A.**

361 The methods  $\mathcal{E}$  and  $\mathcal{G}$  use the centred second-order finite difference approximation  
 362 to the conservation of momentum equation (1b) denoted as  $\mathcal{G}_u$ . For the conservation of  
 363 mass equation (1a)  $\mathcal{E}$  uses the two step Lax-Wendroff method denoted as  $\mathcal{E}_h$  while  $\mathcal{G}$   
 364 uses a centred second-order finite difference approximation denoted as  $\mathcal{G}_h$ .

365     *Appendix A.1.  $\mathcal{G}_u$  for Conservation of Momentum Equation*

366     The finite difference approximation to (1b) on our grid is

$$367 \quad h_i^n u_i^{n+1} - (h_i^n)^2 \left( \frac{u_{i+1}^{n+1} - u_{i-1}^{n+1}}{2\Delta x} \right) - \frac{(h_i^n)^3}{3} \left( \frac{u_{i+1}^{n+1} - 2u_i^{n+1} + u_{i-1}^{n+1}}{\Delta x^2} \right) = -Y_i^n \quad (\text{A.1})$$

369     and

$$370 \quad Y_i^n = 2\Delta t X_i^n - h_i^n u_i^{n-1} + (h_i^n)^2 \left( \frac{u_{i+1}^{n-1} - u_{i-1}^{n-1}}{2\Delta x} \right) + \frac{(h_i^n)^3}{3} \left( \frac{u_{i+1}^{n-1} - 2u_i^{n-1} + u_{i-1}^{n-1}}{\Delta x^2} \right).$$

372     Equation (A.1) can be rearranged into an explicit update scheme  $\mathcal{G}_u$  for  $u$  given its  
373     current and previous values, so that

$$374 \quad \begin{bmatrix} u_0^{n+1} \\ \vdots \\ u_m^{n+1} \end{bmatrix} = A^{-1} \begin{bmatrix} -Y_0^n \\ \vdots \\ -Y_m^n \end{bmatrix} =: \mathcal{G}_u(\mathbf{u}^n, \mathbf{h}^n, \mathbf{u}^{n-1}, \Delta x, \Delta t) \quad (\text{A.2})$$

376     where  $A$  is a tri-diagonal matrix.

377     *Appendix A.2. Numerical Methods for Conservation of Mass Equation*

378     The two step Lax-Wendroff update  $\mathcal{E}_h$  for  $h$  is

$$379 \quad h_{i+1/2}^{n+1/2} = \frac{1}{2} (h_{i+1}^n + h_i^n) - \frac{\Delta t}{2\Delta x} (u_{i+1}^n h_{i+1}^n - h_i^n u_i^n),$$

$$382 \quad h_{i-1/2}^{n+1/2} = \frac{1}{2} (h_i^n + h_{i-1}^n) - \frac{\Delta t}{2\Delta x} (u_i^n h_i^n - h_{i-1}^n u_{i-1}^n)$$

384     and

$$385 \quad h_i^{n+1} = h_i^n - \frac{\Delta t}{\Delta x} (u_{i+1/2}^{n+1/2} h_{i+1/2}^{n+1/2} - u_{i-1/2}^{n+1/2} h_{i-1/2}^{n+1/2}).$$

387     The quantities  $u_{i\pm 1/2}^{n+1/2}$  are calculated using  $u^{n+1}$  obtained by applying  $\mathcal{G}_u$  (A.2) to  $u^n$  then  
388     linearly interpolating in space and time to give

$$389 \quad u_{i+1/2}^{n+1/2} = \frac{u_{i+1}^{n+1} + u_{i+1}^n + u_i^{n+1} + u_i^n}{4}$$

391     and

$$392 \quad u_{i-1/2}^{n+1/2} = \frac{u_i^{n+1} + u_i^n + u_{i-1}^{n+1} + u_{i-1}^n}{4}.$$

394     Thus we have the following update scheme  $\mathcal{E}_h$  for (1a)

$$395 \quad \mathbf{h}^{n+1} = \mathcal{E}_h(\mathbf{u}^n, \mathbf{h}^n, \mathbf{u}^{n+1}, \Delta x, \Delta t). \quad (\text{A.3})$$

397        The second order centered finite difference approximation to the conservation of  
 398        mass equation (1a) is

$$399 \quad h_i^{n+1} = h_i^{n-1} - \Delta t \left( u_i^n \frac{h_{i+1}^n - h_{i-1}^n}{\Delta x} + h_i^n \frac{u_{i+1}^n - u_{i-1}^n}{\Delta x} \right). \\ 400$$

401        Thus we have an update scheme  $\mathcal{G}_h$  for all  $i$

$$402 \quad \mathbf{h}^{n+1} = \mathcal{G}_h(\mathbf{u}^n, \mathbf{h}^n, \mathbf{h}^{n-1}, \Delta x, \Delta t). \quad (\text{A.4}) \\ 403$$

404        *Appendix A.3. Complete Method*

405        The method  $\mathcal{E}$  is the combination of (A.3) for (1a) and (A.2) for (1b) in the follow-  
 406        ing way

$$407 \quad \begin{cases} \mathbf{u}^{n+1} = \mathcal{G}_u(\mathbf{u}^n, \mathbf{h}^n, \mathbf{u}^{n-1}, \Delta x, \Delta t) \\ \mathbf{h}^{n+1} = \mathcal{E}_h(\mathbf{u}^n, \mathbf{h}^n, \mathbf{u}^{n+1}, \Delta x, \Delta t) \end{cases} \quad \mathcal{E}(\mathbf{u}^n, \mathbf{h}^n, \mathbf{u}^{n-1}, \mathbf{h}^{n-1}, \Delta x, \Delta t). \quad (\text{A.5}) \\ 408$$

409        The method  $\mathcal{G}$  is the combination of (A.4) for (1a) and (A.2) for (1b) in the follow-  
 410        ing way

$$411 \quad \begin{cases} \mathbf{h}^{n+1} = \mathcal{G}_h(\mathbf{u}^n, \mathbf{h}^n, \mathbf{h}^{n-1}, \Delta x, \Delta t) \\ \mathbf{u}^{n+1} = \mathcal{G}_u(\mathbf{u}^n, \mathbf{h}^n, \mathbf{u}^{n-1}, \Delta x, \Delta t) \end{cases} \quad \mathcal{G}(\mathbf{u}^n, \mathbf{h}^n, \mathbf{u}^{n-1}, \mathbf{h}^{n-1}, \Delta x, \Delta t). \quad (\text{A.6}) \\ 412$$